Electrospun Sb/C Fibers for a Stable and Fast Sodium-Ion Battery Anode

Yujie Zhu,[†] Xiaogang Han,[‡] Yunhua Xu,[†] Yihang Liu,[†] Shiyou Zheng,[†] Kang Xu,[§] Liangbing Hu,[‡] and Chunsheng Wang[†,*]

[†]Department of Chemical and Biomolecular Engineering and [‡]Department of Materials Science and Engineering, University of Maryland, College Park, Maryland 20742, United States and [§]Electrochemistry Branch, Power and Energy Division Sensor and Electron Devices Directorate, U.S. Army Research Laboratory, Adelphi, Maryland 20783, United States

ABSTRACT Sodium-ion batteries (SIBs) are considered a top alternative to lithium-ion batteries (LIBs) for large-scale renewable energy storage units due to their low cost and the abundance of sodium-bearing precursors in the earth's mineral deposits. However, the development of anode materials for SIBs to date has been mainly limited to carbonaceous materials with minimal research devoted to high capacity alloy-based materials. In this study, an antimony (Sb)/carbon (C) electrode with ~30 nm Sb nanoparticles (NPs) uniformly encapsulated in interconnecting one-dimensional (1D) 400 nm carbon fibers (denoted as SbNP@C) was fabricated using a simple and scalable electrospinning method. This binder-free, current collector-free SbNP@C electrode demonstrated high capacity and stable long-term cycling performance at various current densities. The SbNP@C electrode showed an initial total capacity of 422 mAh/$g_{electrode}$ and retained 350 mAh/$g_{electrode}$ after 300 deep charge–discharge cycles under 100 mA/g_{Sb}. Moreover, because of the efficient 1D sodium-ion transport pathway and the highly conductive network of SbNP@C, the electrode preserved high overall capacities even when cycled at high currents, extending its usability to high power applications.

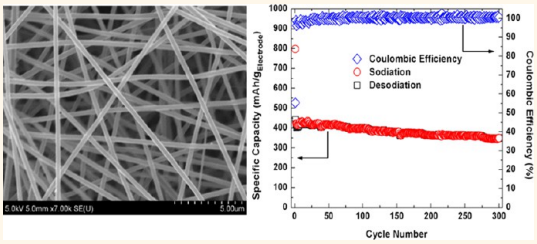

KEYWORDS: electrospinning · antimony · anode · sodium ion battery

Lithium-ion batteries (LIBs) have become one of the most important technologies for energy storage in portable devices and are now industry standards for use in electric/hybrid electric vehicles and renewable energy storage.[1] However, considering the limited and unevenly distributed availability of lithium deposits, cost will become a major issue for future LIB production. As alternatives to LIBs, room temperature sodium-ion batteries (SIBs) have gained increasing attention due to their low cost and the relative abundance of sodium over lithium.[2] Existing SIB research has been largely focused on the development of stable and low cost cathode materials. A wide variety of compounds have been proposed for SIB cathodes, and good progress has been made on a number of these materials.[3−12] For example, Cao *et al.*[13] reported a single crystal $Na_4Mn_9O_{18}$ nanowire cathode, which showed exceptional cycling stability with 77% capacity retention after 1000 charge–discharge cycles. More recently, Goodenough *et al.*[14] proposed a sodium manganese hexacyanoferrate, which demonstrated high-rate performance and could be produced at very low cost.

Compared to the fast development and diversity of cathode materials, innovation in anode materials for SIBs has been relatively slow and mainly limited to nongraphitic carbonaceous materials, since the commercially available graphite anode for LIBs has been shown to have a very low sodium intercalation capacity of 32–35 mAh/g.[15] Various carbonaceous materials, such as coke,[16] carbon black,[17] template carbon,[18] hollow carbon nanowires,[19] hollow carbon nanospheres,[20] and nitrogen-doped porous carbon nanosheets,[21] *etc.*, have been studied. Although several reasonable carbonaceous candidates have been proposed, they were for the most part cycled at relatively low current rates with a specific capacity typically less than 300 mAh/g. Also, most of them possessed porous and/or hollow structures, and sodium storage in these materials usually involved filling the nanoscopic pores in the carbon.[22] Given the intrinsic low tap density of carbonaceous materials, the porous/hollow structure

* Address correspondence to cswang@umd.edu.

Received for review May 21, 2013 and accepted June 26, 2013.

Published online June 26, 2013
10.1021/nn4025674

results in even lower volumetric energy densities, which limited the applicability of these materials.

On the other hand, alloy-based materials usually provided much higher gravimetric and volumetric specific capacities compared to carbonaceous materials. Although high-capacity alloying anodes have undergone intensive development for LIBs, little research has been done for alloy-based anode materials for SIBs. For LIBs, the rapid capacity decay of alloy-based materials (Si, Sn, *etc.*) has been attributed to the lithiation-/delithiation-induced volume change. Since the sodium ion possesses a larger radius than the lithium ion, the effect of volume change upon sodiation/desodiation should be even more severe for the application of alloy-based materials in SIBs.[23] Thus, the development of stable alloy-based anode materials for SIBs became more challenging than for LIBs.[23,24] Up until now, only a few alloy-based materials or their compounds, such as Sn,[25−27] SnSb,[28] Cu_2Sb,[29] and Sb_2O_4,[30] have been investigated. Among all reported alloy-based materials, antimony (Sb), with a high theoretical capacity of 660 mAh/g, seems to be the best anode candidate for SIBs. As recently reported by Qian *et al.*,[31] Sb/carbon nanocomposite, synthesized by a simple ball-milling method, showed a reversible Na storage capacity of 610 mAh/g and retained 94% of its initial capacity after 100 charge−discharge cycles. Darwiche *et al.*[32] showed that good cycling performance can even be achieved using bulk Sb and suggested the sodiation/desodiation process in Sb involved an amorphous intermediate phase that was sharply different from the lithiation/delithiation process in the same material. However, stable cycling performance of Sb can only be realized by using an electrolyte with a fluoroethylene carbonate (FEC) additive, which has been shown to improve the stability of the solid electrolyte interface (SEI) film. The Sb electrode without FEC additive will not survive for more than 20−50 cycles.[31,32] Even for electrodes cycled in cells using FEC in the electrolyte, the long-term cycling stability of Sb (>160 charge−discharge cycles) has never been reported, especially for high currents charge/discharge.

Herein, we report a Sb/carbon electrode with a novel 1D nanostructure, in which Sb nanoparticles (NPs) were uniformly encapsulated in interconnecting carbon fibers. This novel 1D nanostructure (SbNP@C) with Sb nanoparticles buffered by a carbon matrix can effectively tolerate the massive volume changes during the Na alloying/dealloying reaction. The SbNP@C electrode was generated using an inexpensive, simple, and scalable electrospinning process. The electrospun free-standing nanofiber mats were directly used as electrodes in sodium batteries without the use of binder, carbon black, or a metal current collector, which greatly reduced the inactive weight and cost of the cells. Because of the unique nanostructure, long-term, and stable cycling performance (>300 deep charge−discharge cycles) at both low and high current rates with high overall capacities was achieved for the first time, and our results demonstrated that a stable cycling performance of Sb can be realized using an FEC-free electrolyte. Moreover, the highly conductive network of the SbNP@C electrode allowed it to be cycled at ultrahigh current rates and still maintain considerably high overall capacities, which make it suitable for high power applications.

RESULTS AND DISCUSSION

Figure 1 schematically illustrates the experimental procedures. The precursor solution of $SbCl_3$ and polyacrylonitrile (PAN) was first electrospun into a fiber matrix (Figure 1a). The as-spun fibers (Figure 1a) were then stabilized in air at 250 °C. Afterward, the stabilized fibers (Figure 1b) were thermally treated in an Ar/H_2 atmosphere at 600 °C. During the heat treatment, the PAN carbonized and $SbCl_3$ decomposed to Sb NPs embedded in carbon fibers. The carbonized fiber matrix (Figure 1c) was then cut into electrodes, and these free-standing electrodes were directly used for assembling sodium cells. Neither mechanical milling nor slurry casting was needed to prepare the electrodes. More experimental details can be found in the Methods section.

Figure 2 shows the scanning electron microscopy (SEM) images for the as-spun (Figure 2a,b) and carbonized fibers (Figure 2c−f). As shown in Figure 2 panels a and b, the as-spun PAN/$SbCl_3$ fibers are long and continuous with a uniform diameter. The carbonized fibers maintained their fibrous morphology with no obvious diameter change compared to the as-spun fibers. Figure 2 panels e and f show high magnification SEM images of the carbonized fibers. The obtained fibers have a smooth surface and show an interconnecting network. No Sb particles were found on the surface of the fibers, suggesting all Sb particles were encapsulated in the carbon fibers. This unique 1D nanostructure, along with the interconnecting nature of the fibers, facilitated both fast electronic and ionic transport. The crystal structure of the SbNP@C sample was studied using powder X-ray diffraction (XRD) (Figure S1, Supporting Information (SI)). The XRD pattern in Figure S1 was well indexed with crystal antimony (JCPDS card No.: 05-0562) without any detectable impurity.

Transmission electron microscopy (TEM) (Figure 3) was further used to investigate the encapsulation of Sb NPs in the carbon fibers. Since the carbonization temperature was set to 600 °C, which is below the melting point of Sb (631 °C), it effectively prevented the aggregation of Sb NPs during heat treatment. As shown in Figure 3a, the Sb NPs, with particle sizes ranging from 20 to 50 nm, were well dispersed inside the carbon fibers with carbon separating individual Sb NPs. The high resolution TEM (HRTEM) image in Figure 3b reveals the fine lattice fringe and crystalline

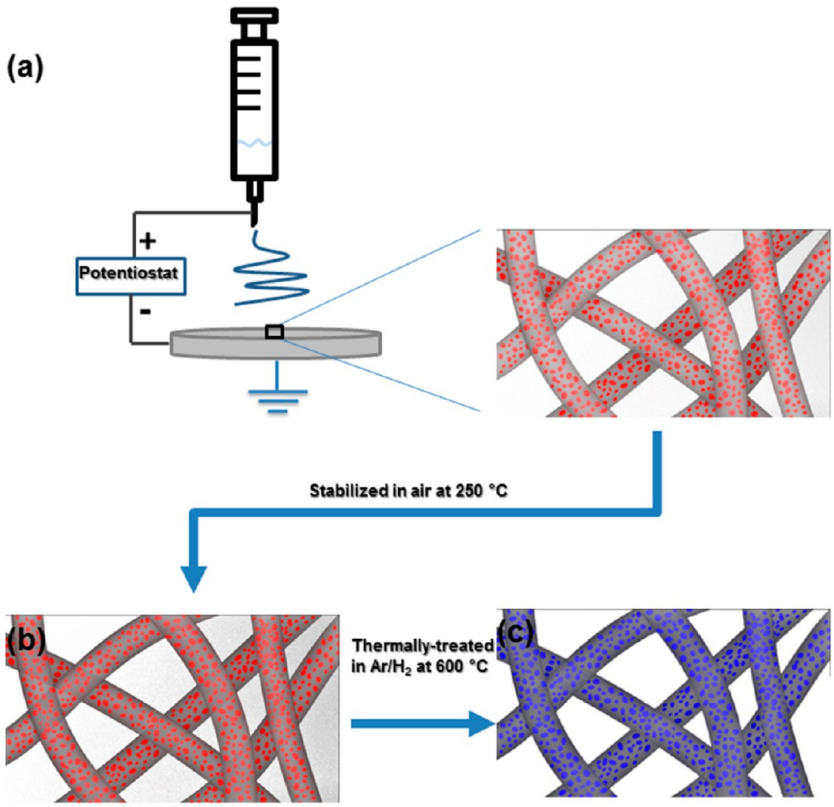

Figure 1. Schematic illustration of the synthesis process for the SbNP@C electrode.

nature of a single Sb NP, which is consistent with the XRD result (Figure S1, SI). Figure 3 panels c–e show the bright-field TEM image (Figure 3c) of one fiber and its energy dispersive X-ray spectroscopy (EDS) element mapping for Sb (Figure 3d) and carbon (Figure 3e). As revealed by the EDS element mapping, Sb NPs were uniformly distributed and entirely confined in the core of the carbon fiber.

The Sb/carbon ratio in the fibers was determined using thermogravimetric analysis (TGA) (Figure S2, SI). The slight weight loss around 100 °C is due to water evaporation. The weight loss around 500 °C is mainly attributed to the oxidation of carbon, and the subsequent weight gain after 500 °C might be due to the oxidation of Sb NPs. On the basis of the TGA result, the Sb content in the SbNP@C composite was estimated to be 54 wt %.

The SbNP@C fibers were directly used as electrodes and assembled in sodium coin cells with FEC-free electrolyte (1.0 M $NaClO_4$ in ethylene carbonate (EC): dimethyl carbonate (DMC), 1:1 by volume), and the electrochemical performance of the SbNP@C electrodes was first investigated using cyclic voltammetry (CV). Figure 4a shows the CV results of the initial five cycles at a scan rate of 0.1 mV/s between 0 and 2 V (vs Na/Na^+). Two current peaks occurred around 0.42 and 0.11 V during the first sodiation scan and shifted to 0.45 and 0.25 V in the second sodiation scan. The two current peaks at 0.45 and 0.25 V were attributed to the formation of NaSb and Na_3Sb, respectively.[31] The peak current at 0.42 V *versus* Na/Na^+ in the first sodiation scan is higher than the peak current at 0.45 V in the second scan primarily due to the decomposition of the liquid electrolyte and formation of an SEI layer on the surface of the carbon fibers during the first scan,[19−21] which was also observed in sodium cells with carbon fiber electrodes (Figure S3a, SI). The current peak at 0.11 V *versus* Na/Na^+ is jointly due to sodium alloying with Sb at 0.25 V and insertion into the carbonaceous materials near 0.0 V. For the cell with a carbon fiber electrode, the CV scan showed a sharp sodium insertion peak around 0.0 V (Figure S3a, SI), which was also observed in other carbon-based materials.[19−21] The reduced current peak at 0.11 V in the second sodiation scan was mainly due to the capacity decay of carbon in the second cycle (Figure S3a, SI). The first oxidation scan presented one clear current peak at 0.8 V *versus* Na/Na^+. Previous studies showed that Sb/carbon composites presented two distinct current peaks at 0.77 and 0.90 V *versus* Na/Na^+ during the oxidation scan,[31] which correspond to the desodiation of Na_3Sb and NaSb, respectively. The two peak currents appeared to merge into one broad peak in this study, which might be caused by a differing carbon content and dissimilar sizes of Sb particles between previous studies and the present one, as suggested by Darwiche *et al.*[32] The desodiation peak gradually shifted to higher potentials

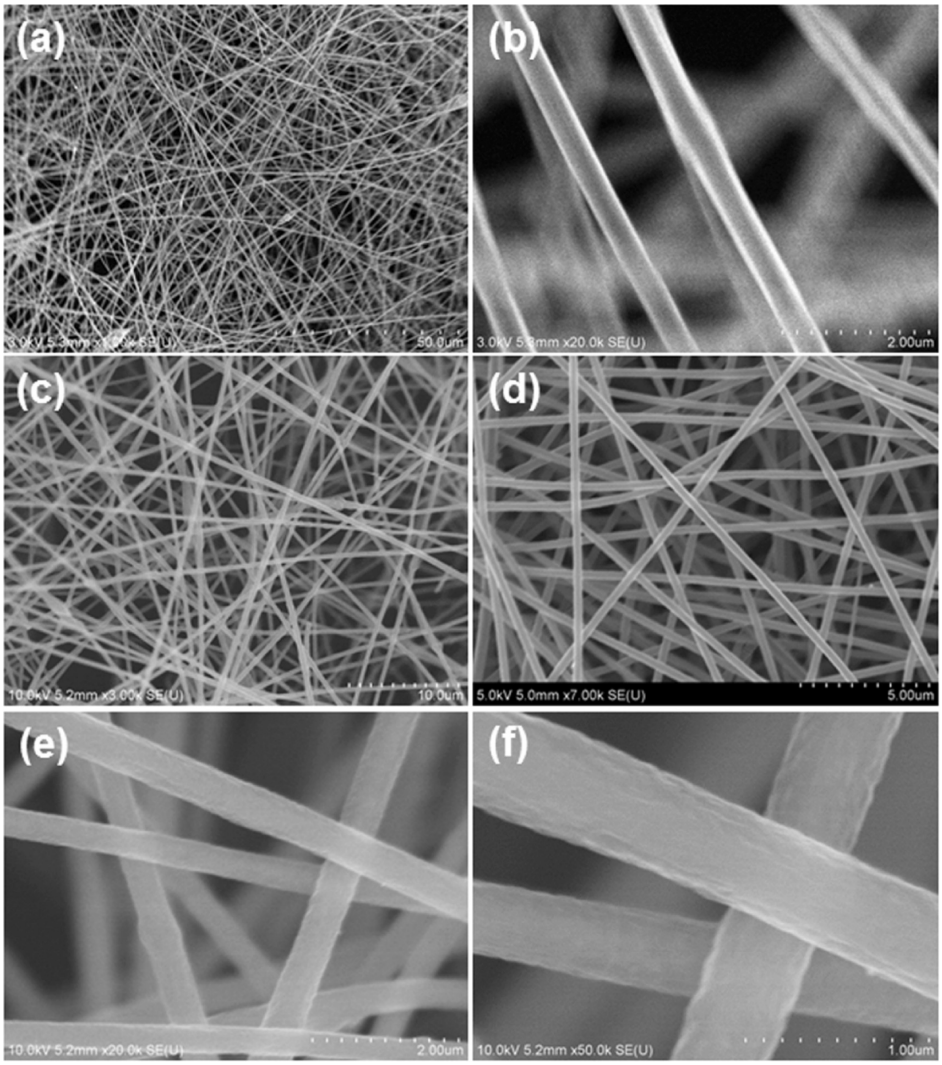

Figure 2. SEM images of as-spun PAN/$SbCl_3$ fibers (a, b) and the carbonized fibers (c–f).

during the second and subsequent scans, indicating higher polarization, while no significant changes were observed for the reduction peak between the second and subsequent scans. After the fourth reduction–oxidation scan, the CV curves showed negligible change. The differences observed during the initial few cycles might be caused by local structure rearrangement in the electrode to accommodate the strain/stress induced during sodiation/desodiation, which was also observed during the lithiation/delithiation of some alloy-based anodes in LIBs.[33]

The electrochemical cycling stability of the SbNP@C electrode in the sodium cells was tested under galvanostatic conditions. Figure 4b shows the charge–discharge curves of the SbNP@C electrode under a constant current density of 100 mA/g_{Sb}. The current densities in this study were calculated based on the mass of Sb in the composite. However, to realize the advantages of our free-standing SbNP@C electrode, all of the capacities in this study were calculated on the basis of total weight of the working electrode (Sb+carbon). As shown in Figure 4b, the voltage profiles showed sloping lines during both charge and discharge, which were consistent with the broad current peaks observed during CV scans. The sodiation capacity for the first cycle was 800 mAh/$g_{electrode}$ with a Coulombic efficiency around 55%. Such a low efficiency of the first cycle was mainly attributed to the irreversible formation of the SEI film on the surface of the carbon fibers during the first sodiation process, which was also observed for the carbon fiber electrode (Sb-free) during the first sodiation process (Figure S3b, SI). The sodiation capacity of the second cycle was around 422 mAh/$g_{Electrode}$. Since carbon fibers can only provide a sodiation capacity of 160 mAh/g_{Carbon} (Figure S3b, SI) at the same current density, the capacity contributed by Sb NPs was around 640 mAh/g_{Sb}, which was very close to its theoretical sodium storage capacity (660 mAh/g_{Sb} corresponding to a formula of Na_3Sb), demonstrating the full utilization of Sb NPs. The Coulombic efficiency of the second cycle exceeded 98% and remained stable for the rest of the

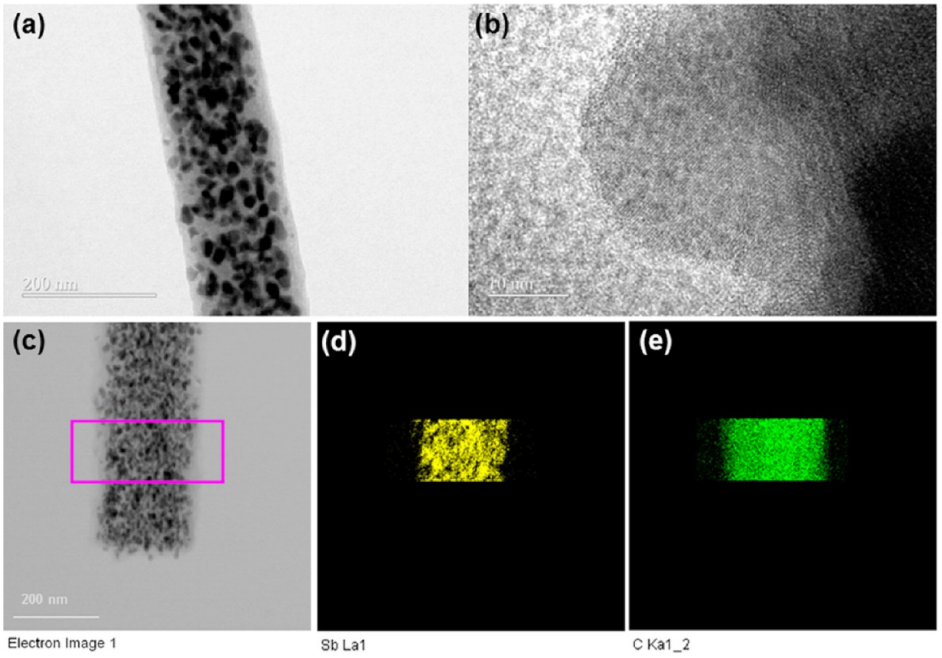

Figure 3. (a) TEM image of carbon-encapsulated Sb fibers. (b) High resolution TEM image of one Sb NP. (c) TEM image of one carbonized fiber. (d, e) The EDS elemental mapping of the area, marked by the purple rectangle in image c, for Sb (d) and carbon (e).

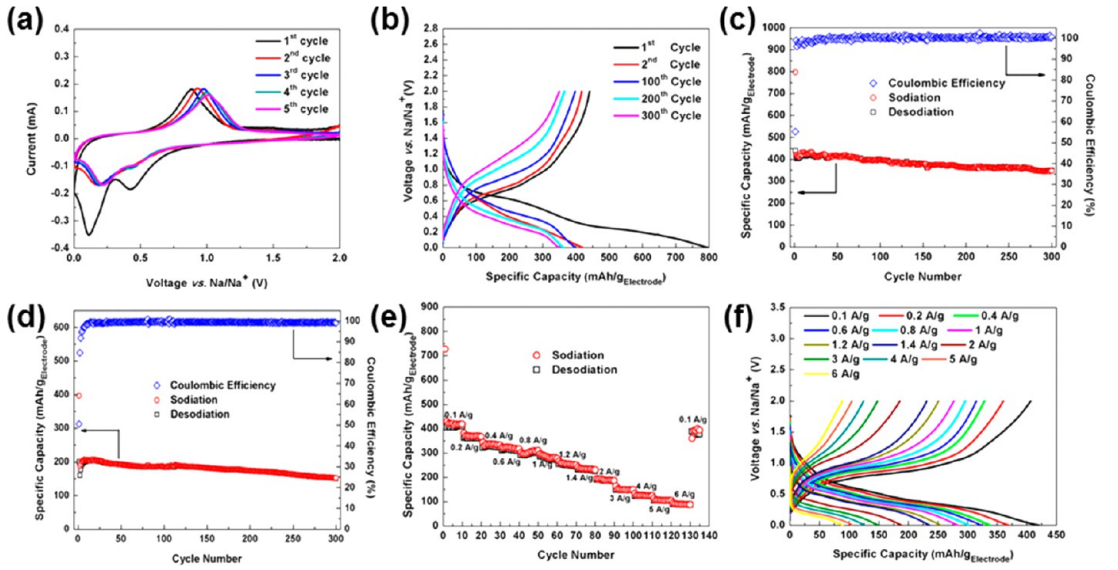

Figure 4. Electrochemical characterizations and cell performance of the SbNP@C electrode as the anode material for Na-ion batteries. (a) Cyclic voltammetry of the SbNP@C electrode between 0 and 2 V at a scanning rate of 0.1 mV/s. (b) Galvanostatic charge/discharge voltage profiles of the 1st, 2nd, and later cycles of SbNP@C electrode under a current density of 0.1 A/g_{Sb}. (c) Cycle performance of SbNP@C electrode at a current density of 0.1 A/g_{Sb}. (d) Cycle performance of SbNP@C electrode at a current density of 2 A/g_{Sb}. (e) Charge/discharge capacity and (f) voltage profiles of the SbNP@C electrode cycled at various current densities from 0.1 A/g_{Sb} to 6 A/g_{Sb}. Note: The electrolyte used here was 1.0 M $NaClO_4$ in ethylene carbonate (EC): dimethyl carbonate (DMC) (1:1 by volume) liquid electrolyte and the specific capacities were calculated on the basis of total mass of working electrode.

cycles. As shown in Figure 4c, the SbNP@C electrode exhibited excellent cycling performance. After 300 deep charge−discharge cycles under a current density of 100 mA/g_{Sb}, the SbNP@C electrode still maintained an overall desodiation capacity of 350 mAh/$g_{electrode}$, which was much higher than the capacity of the best carbonaceous anode materials reported to date after similar charge−discharge cycles.

The capacity decay in Figure 4c was very slow, at only 0.06% decay per cycle compared with the first desodiation capacity. Previous studies showed that the stable cycling of sodiation/desodiation in Sb can only be achieved using an electrolyte with FEC additive used to improve the stability of the SEI film.[31,32] For comparison, the SbNP@C electrode was also tested in EC/DMC electrolyte (1:1 by volume) with FEC additive

in sodium cells (Figure S4, SI). The sodium cell with FEC electrolyte showed similar cycling stability as the FEC-free cells, demonstrating the effectiveness of the SbNP@C electrode's microstructure in stabilizing the SEI film.

The SbNP@C not only showed stable cycling performance at a low current density but also demonstrated good cycle life under a high current density. Figure 4d shows the cycling performance of the SbNP@C electrode at a high current density of 2 A/g_{Sb}. In contrast to results for low current charge−discharge (Figure 4c), the Coulombic efficiency of the initial few cycles for the high current charge−discharge was low, but it reached over 99% after few charge−discharge cycles. Surprisingly, the SbNP@C electrode displayed great cycling stability at a high charge−discharge current rate, with 92% of its initial capacity retained after 100 cycles and 75% after 300 cycles.

The rate performance of SbNP@C electrode was tested in sodium cells, and the results are shown in Figure 4e. The SbNP@C electrode displayed outstanding high rate capability and can be reversibly cycled at a high current density of 6 A/g_{Sb}, which roughly corresponds to a C-rate as high as 10 C, considering the theoretical sodium storage capacity in Sb of 660 mAh/g. As shown in Figure 4e, the SbNP@C electrode can deliver total reversible capacities of 405, 360, 323, 310, 300, 273, 250, 230, 185, 146, 123, 104, and 88 mAh/$g_{electrode}$ at the current densities of 0.1, 0.2, 0.4, 0.6, 0.8, 1.0, 1.2, 1.4, 2.0, 3.0, 4.0, 5.0, and 6.0 A/g_{Sb}. For comparison, the carbon fiber electrode (Sb-free) was also tested under different current densities (Figure S5, SI). When the current density was higher than 0.8 A/g, the carbon fiber electrode provided negligible sodium storage capacities (Figure S5, SI), so it can be concluded that for current densities higher than 0.8 A/g, the capacities were entirely attributable to the Sb NPs. Also shown in Figure 4e, when the current was switched from 6 A/g_{Sb} to 0.1 A/g_{Sb} after 130 charge−discharge cycles, the capacity almost fully recovered, indicating the stability of the electrode under a wide range of current densities. Figure 4f shows the charge−discharge voltage profiles of the SbNP@C electrode under different current densities. A 400 mV voltage offset, defined as the voltage difference between sodiation and desodiation at the same state-of-charge, existed at 50% state-of-charge under the current density of 0.1 A/g_{Sb}. As current density increased from 0.1 A/g_{Sb} to 6.0 A/g_{Sb}, the charge−discharge voltage profiles had similar shapes, with increasing of the voltage offset. As shown by Sethuraman *et al.*[34,35] for Si thin film electrode in LIBs, the physical origins for the voltage offset were mainly attributed to polarization losses and mechanical energy dissipation caused by charge−discharge induced stress effect. The voltage offset will lower the energy efficiency of the cell and can be minimized by further improving the kinetics of the electrode.[36]

To investigate the mechanism for the good cycling stability and structure change of the SbNP@C electrode, the sodium cell tested in Figure 4c was disassembled after 300 discharge/charge cycles in the fully desodiated condition, and the micromorphology of the SbNP@C electrode was studied using both SEM and TEM. Before taking the images, the after-cycled electrode was rinsed with propylene carbonate (PC) to remove the $NaClO_4$ residue on the fibers. Figure 5 panels a and b show the digital images of one after-cycled SbNP@C electrode. The after-cycled SbNP@C electrode still maintained its structural integrity (Figure 5a) and flexibility (Figure 5b). The SEM images in Figure 5c,d show that an SEI film covered the SbNP@C, which might be the reason accounting for the gradual capacity decay observed in Figure 4c. However, in the high magnification SEM image (Figure 5d), the long, continuous, and robust fibers in the SbNP@C electrode can still be clearly observed even after 300 discharge/charge cycles, and no broken fibers were observed, indicating the strong structural fortitude of the SbNP@C electrode against sodiation/desodiation.

Figure 6 shows the TEM images and the EDS element mapping for the after-cycled fibers in the SbNP@C electrode. The diameter of the fibers was very uniform (Figure 6a) and similar to that of the uncycled fibers (Figure 2), suggesting that this electrode structure can effectively accommodate the volume change during sodiation/desodiation. After 300 discharge/charge cycles, the Sb NPs seemed to break into smaller particles and transformed from crystalline to amorphous, as evidenced by Figure 6b, in which the after-cycled Sb NPs generally consisted of secondary particles, and the electron diffraction pattern (Figure S6, SI) of the after-cycled fiber, respectively. Moreover, as shown by the TEM image of one after-cycled fiber (Figure 6c) and its EDS element mapping of Sb (Figures 6d) and carbon (Figure 6e), after a sustainable number of cycles, Sb NPs still remained confined in the core of the carbon fiber, indicating the mechanical stability of the fibers.

The charge/discharge process in alloy-based anode materials was often accompanied by a large volume change. For regular electrodes with metal current collectors, binder, and conductive additives, this huge volume change could cause pulverization, resulting in a loss of contact between active materials and current collector/conductive additives. This is considered to be the major reason for the capacity decay in these materials.[37] The excellent cycling performance of the SbNP@C electrode can be ascribed to its unique microstructure, in which the Sb NPs are encapsulated in the carbon fibers, and the carbon fibers themselves serve as both current collector and conductive material. Although the Sb NPs might expand, shrink, or even crack during sodiation/desodiation, they were still confined inside the carbon fibers. Moreover, the small size of the Sb NPs in the carbon fibers reduced the

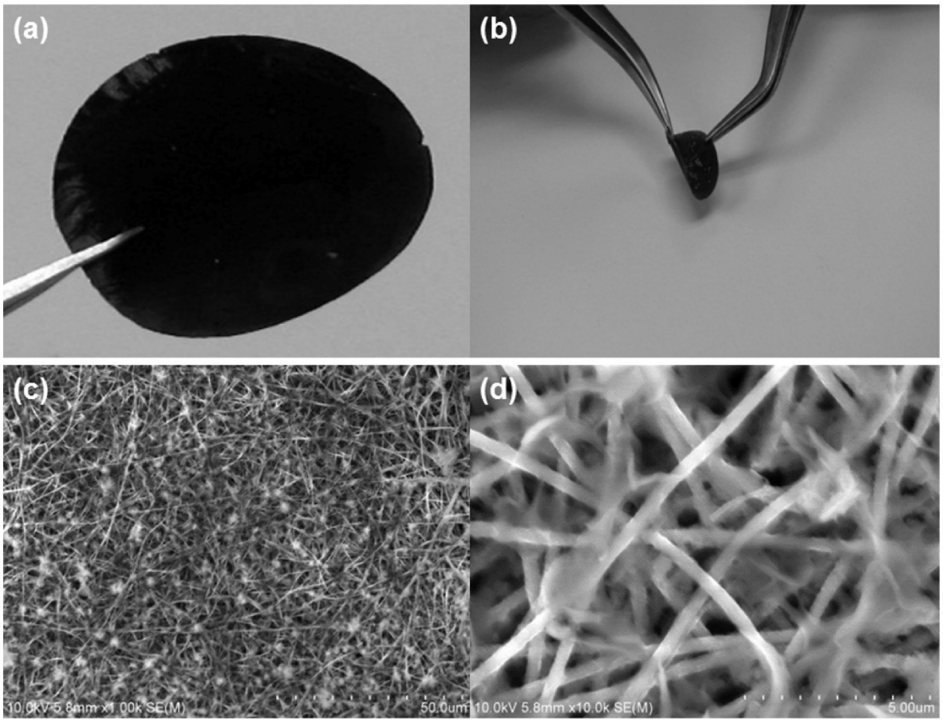

Figure 5. Digital (a, b) and SEM images (c, d) of the SbNP@C electrode after 300 charge−discharge cycles. Note: The cell was disassembled at the fully desodiated state.

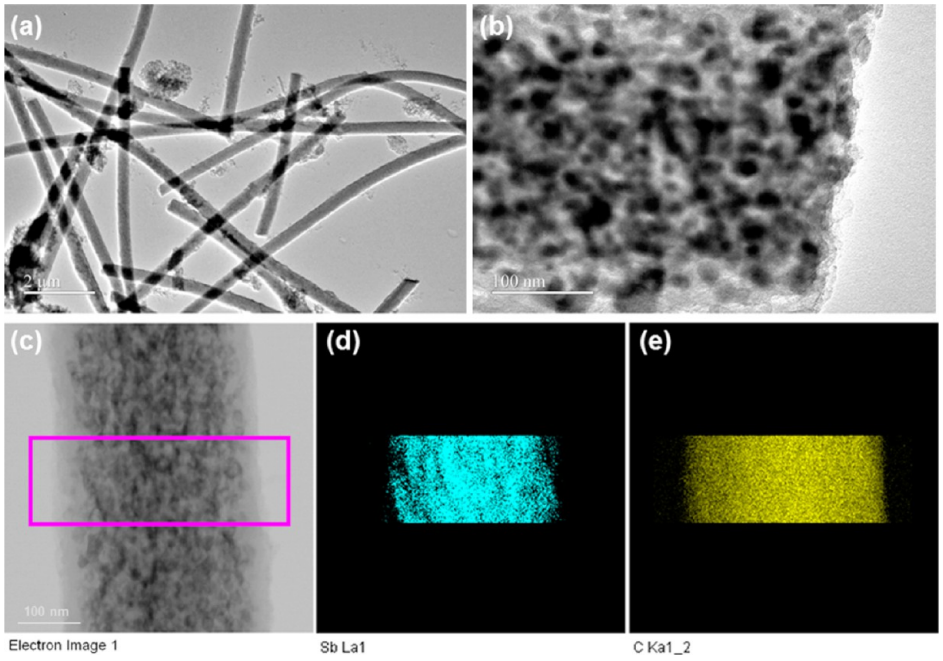

Figure 6. (a, b) TEM images for the after-cycled fibers in the SbNP@C electrode. (c) TEM image of one after-cycled fiber. (d, e) The EDS elemental mapping of the area, marked by the purple rectangle in image c, for Sb (d) and carbon (e).

absolute strain, prevented pulverization, and preserved electrode integrity. The electrode's exceptional rate performance can be attributed to the efficient 1D electronic transport pathway. Also, the carbon fibers encapsulated and connected individual Sb NPs together to form a highly conductive network, which provided both fast electronic and ionic transport.

CONCLUSION

The development of high capacity alloy-based anodes for SIBs is still in its incipient stages, but it is the authors' hope that this research is a quantifiable step forward toward realization of marketable sodium-ion rechargeable batteries. In this study, a novel SbNP@C electrode with 1D nanostructure was synthesized using

a simple electrospinning method. In the SbNP@C electrode, Sb NPs were well dispersed and confined to the core of the 1D carbon fibers. The electrode demonstrated excellent cycling stability with high overall capacities at both low and high current rates, and its strong structural integrity was able to withstand the sodiation/desodiation induced volume change. Moreover, due to the unique 1D morphology and conductive network, the SbNP@C electrodes displayed exceptional high rate capability, allowing its use in high power applications.

METHODS

Synthesis of SbNP@C Electrode. An amount of 1.369 g of antimony chloride ($SbCl_3$, Sigma-Aldrich) was first dissolved into 10 mL of *N,N*-dimethylformamide (DMF) with a concentration of 0.6 M. Then, 0.65 g of polyacrylonitrile (PAN) was added to the solution with vigorous stirring for 3 h. The obtained mixture was used as the precursor solution for electrospinning.

The precursor solution was loaded into a plastic syringe connected to a blunt-tip needle, which was connected to a syringe pump. The flow rate of the solution was set to be 10 μL/min. A grounded stainless steel plate was used to collect the fibers, and the distance between the needle and the fiber collector was set to be 15 cm. A voltage of 10 kV was applied between the needle and the plate to initiate the electrospinning.

The as-collected fibers were first stabilized in air at 250 °C for 60 min with a heating rate of 10 °C/min. Then, the fibers were carbonized in a tube furnace at 600 °C for 5 h under H_2 (5 vol %)/Ar (95 vol %) atmosphere with a heating rate of 2 °C/min to obtain the SbNP@C electrode material.

Material Characterizations. The crystal structure of the fibers was characterized using powder X-ray diffraction (XRD) on a D8 Advanced with LynxEye and SolX (Bruker AXS, WI, USA) using a CuKα radiation source operated at 40 kV and 40 mA. The morphology of the fibers was characterized using both Hitachi SU-70 analytical ultra-high-resolution scanning electron microscopy (SEM) and JEOL 2100F field emission transmission electron microscopy (TEM) at the NanoCenter at the University of Maryland. The after-cycled electrode shown in Figures 5 and 6, was rinsed with propylene carbonate (PC) before taking the images. Thermogravimetric analysis (TGA) was used to determine the percentage of carbon in the fiber sample. The powder sample was loaded into the TGA equipment (CAHN TG 2131, USA) and heated from room temperature to 800 °C in an air atmosphere with a heating rate of 10 °C/min.

Electrochemical Characterizations. The heat-treated fiber mats were cut into electrodes, which were directly assembled into sodium cells without mechanical milling or slurry coating processes. Neither a metal current collector nor additives (conductive carbon, binder, *etc.*) were needed. The electrode was first dried in a vacuum oven at 100 °C overnight. Na coin cells assembled with a Na foil counter electrode, a SbNP@C working electrode, Celgard 3501 microporous film separators, and 1.0 M $NaClO_4$ in ethylene carbonate (EC):dimethyl carbonate (DMC) (1:1 by volume) liquid electrolyte were used for electrochemical measurements. The loading weight of the SbNP@C electrode was about 3 mg. For comparison, cells assembled using electrolyte with 5% fluoroethylene carbonate (FEC) additive were also tested.

Galvanostatic charge−discharge tests were performed on an *Arbin* battery test station (BT2000, Arbin Instruments, USA). The cells were cycled between 0 and 2 V under different current densities. All of the current densities used in this study were calculated based on the mass of Sb. After the cell reached the cutoff voltages, it was relaxed for 5 min before subsequent charge or discharge. Cyclic voltammetry (CV) testing with voltages ranging from 0 to 2 V under a scan rate of 0.1 mV/s was recorded using the Solatron 1260/1287 Electrochemical Interface (Solatron Metrology, UK).

Conflict of Interest: The authors declare no competing financial interest.

Acknowledgment. The authors acknowledge the financial support of the National Science Foundation under Contract No. CBET0933228 (Dr. M. Burka, Program Director) and the technical support of the NanoCenter at the University of Maryland.

Supporting Information Available: The XRD pattern of the SbNP@C electrode, the TGA result of the SbNP@C electrode, cyclic voltammograms and charge−discharge voltage profiles of the carbon fiber electrode, cycling performance of the SbNP@C electrode with FEC electrolyte, charge−discharge profiles of the carbon fiber electrode under different current densities, and electron diffraction patterns of the after-cycled fiber. This material is available free of charge *via* the Internet at http://pubs.acs.org.

REFERENCES AND NOTES

1. Tarascon, J.-M.; Armand, M. Issues and Challenges Facing Rechargeable Lithium Batteries. *Nature* **2001**, *414*, 359–367.
2. Palomares, V.; Serras, P.; Villaluenga, I.; Hueso, K. B.; Carretero-Gonzalez, J.; Rojo, T. Na-Ion Batteries, Recent Advances and Present Challenges To Become Low Cost Energy Storage Systems. *Energy Environ. Sci.* **2012**, *5*, 5884–5901.
3. Tarascon, J.-M.; Hull, G. W. Sodium Intercalation into the Layer Oxides $Na_xMo_2O_4$. *Solid State Ionic* **1986**, *22*, 85–96.
4. Doeff, M. M.; Peng, M. Y.; Ma, Y.; De Jonghe, L. C. Orthorhombic Na_xMnO_2 as a Cathode Material for Secondary Sodium and Lithium Polymer Batteries. *J. Electrochem. Soc.* **1994**, *141*, L145–L147.
5. Doeff, M. M.; Richardson, T. J.; Kepley, L. Lithium Insertion Processes of Orthorhombic Na_xMnO_2-Based Electrode Materials. *J. Electrochem. Soc.* **1996**, *143*, 2507–2516.
6. Thackeray, M. M. Manganese Oxides for Lithium Batteries. *Prog. Solid State Chem.* **1997**, *25*, 1–71.
7. Lu, Z.; Dahn, J. R. *In Situ* X-ray Diffraction Study of P2-$Na_{2/3}[Ni_{1/3}Mn_{2/3}]O_2$. *J. Electrochem. Soc.* **2001**, *148*, A1225–A1229.
8. Barker, J.; Saidi, M. Y.; Swoyer, J. L. A Sodium-Ion Cell Based on the Fluorophosphate Compound $NaVPO_4F$. *Electrochem. Solid-State Lett.* **2003**, *6*, A1–A4.
9. Sauvage, F.; Laffont, L.; Tarascon, J.-M.; Baudrin, E. Study of the Insertion/Deinsertion Mechanism of Sodium into $Na_{0.44}MnO_2$. *Inorg. Chem.* **2007**, *46*, 3289–3294.
10. Ellis, B. L.; Makahnouk, W. R. M.; Makimura, Y.; Toghill, K.; Nazar, L. F. A Multifunctional 3.5 V Iron-Based Phosphate Cathode for Rechargeable Batteries. *Nat. Mater.* **2007**, *6*, 749–753.
11. Berthelot, R.; Carlier, D.; Delmas, C. Electrochemical Investigation of the P2-Na_xCoO_2 Phase Diagram. *Nat. Mater.* **2011**, *10*, 74–80.
12. Zhu, Y.; Xu, Y.; Liu, Y.; Luo, C.; Wang, C. Comparison of Electrochemical Performances of Olivine $NaFePO_4$ in Sodium-Ion Batteries and Olivine $LiFePO_4$ in Lithium-Ion Batteries. *Nanoscale* **2013**, *5*, 780–787.
13. Cao, Y.; Xiao, L.; Wang, W.; Choi, D.; Nie, Z.; Yu, J.; Saraf, L. V.; Yang, Z.; Liu, J. Reversible Sodium Ion Insertion in Single Crystalline Manganese Oxide Nanowires with Long Cycle Life. *Adv. Mater.* **2011**, *23*, 3155–3160.
14. Wang, L.; Lu, Y.; Liu, J.; Xu, M.; Cheng, J.; Zhang, D.; Goodenough, J. B. A Superior Low-Cost Cathode for a Na-Ion Battery. *Angew. Chem., Int. Ed.* **2013**, *52*, 1964–1967.
15. Ge, P.; Fouletier, M. Electrochemical Intercalation of Sodium in Graphite. *Solid State Ionics* **1988**, *28−30*, 1172–1175.
16. Doeff, M. M.; Ma, Y.; Visco, S. J.; De Jonghe, L. C. Electrochemical Insertion of Sodium into Carbon. *J. Electrochem. Soc.* **1993**, *140*, L169–L170.
17. Alcántara, R.; Jiménez-Mateo, J. M.; Lavela, P.; Tirado, J. L. Carbon Black: A Promising Electrode Material for Sodium-Ion Batteries. *Electrochem. Commun.* **2001**, *3*, 639–642.

18. Wenzel, S.; Hara, T.; Janek, J.; Adelhelm, P. Room-Temperature Sodium-Ion Batteries: Improving the Rate Capability of Carbon Anode Materials by Templating Strategies. *Energy Environ. Sci.* **2011**, *4*, 3342–3345.
19. Cao, Y.; Xiao, L.; Sushko, M. L.; Wang, W.; Schwenzer, B.; Xiao, J.; Nie, Z.; Saraf, L. V.; Yang, Z.; Liu, J. Sodium Ion Insertion in Hollow Carbon Nanowires for Battery Applications. *Nano Lett.* **2012**, *12*, 3783–3787.
20. Tang, K.; Fu, L.; White, R. J.; Yu, L.; Titirici, M.-M.; Antonietti, M.; Maier, J. Hollow Carbon Nanospheres with Superior Rate Capability for Sodium-Based Batteries. *Adv. Energy Mater.* **2012**, *2*, 873–877.
21. Wang, H.-G.; Wu, Z.; Meng, F.-L.; Ma, D.-L.; Huang, X.-L.; Wang, L.-M.; Zhang, X.-B. Nitrogen-Doped Porous Carbon Nanosheets as Low-Cost, High-Performance Anode Material for Sodium-Ion Batteries. *ChemSusChem* **2013**, *6*, 56–60.
22. Kim, S.-W.; Seo, D.-H.; Ma, X.; Ceder, G.; Kang, K. Electrode Materials for Rechargeable Sodium-Ion Batteries: Potential Alternatives to Current Lithium-Ion Batteries. *Adv. Energy Mater.* **2012**, *2*, 710–721.
23. Chevrier, V. L.; Ceder, G. Challenges for Na-Ion Negative Electrodes. *J. Electrochem. Soc.* **2011**, *158*, A1011–A1014.
24. Ellis, B. L.; Nazar, L. F. Sodium and Sodium-Ion Energy Storage Batteries. *Curr. Opin. Solid State Mater. Sci.* **2012**, *16*, 168–177.
25. Ellis, L. D.; Hatchard, T. D.; Obrovac, M. N. Reversible Insertion of Sodium in Tin. *J. Electrochem. Soc.* **2012**, *159*, A1801–A1805.
26. Xu, Y.; Zhu, Y.; Liu, Y.; Wang, C. Electrochemical Performance of Porous Carbon/Tin Composite Anodes for Sodium-Ion and Lithium-Ion Batteries. *Adv. Energy Mater.* **2013**, *3*, 128–133.
27. Datta, M. K.; Epur, R.; Saha, P.; Kadakia, K.; Park, S. K.; Kumta, P. N. Tin and Graphite Based Nanocomposites: Potential Anode for Sodium Ion Batteries. *J. Power Sources* **2013**, *225*, 316–322.
28. Xiao, L.; Cao, Y.; Xiao, J.; Wang, W.; Kovarik, L.; Nie, Z.; Liu, J. High Capacity, Reversible Alloying Reactions in SnSb/C Nanocomposites for Na-Ion Battery Applications. *Chem. Commun.* **2012**, *48*, 3321–3323.
29. Baggetto, L.; Allcorn, E.; Manthiram, A.; Veith, G. M. Cu_2Sb Thin Film as Anode for Na-Ion Batteries. *Electrochem. Commun.* **2013**, *27*, 168–171.
30. Sun, Q.; Ren, Q.-Q.; Li, H.; Fu, Z.-W. High Capacity Sb_2O_4 Thin Film Electrodes for Rechargeable Sodium Battery. *Electrochem. Commun.* **2011**, *13*, 1462–1464.
31. Qian, J.; Chen, Y.; Wu, L.; Cao, Y.; Ai, X.; Yang, H. High Capacity Na-Storage and Superior Cyclability of Nanocomposite Sb/C Anode for Na-Ion Batteries. *Chem. Commun.* **2012**, *48*, 7070–7072.
32. Darwiche, A.; Marino, C.; Sougrati, M. T.; Fraisse, B.; Stievano, L.; Monconduit, L. Better Cycling Performances of Bulk Sb in Na-Ion Batteries Compared to Li-Ion Systems: An Unexpected Electrochemical Mechanism. *J. Am. Chem. Soc.* **2012**, *134*), 20805–20811.
33. Xu, Y.; Guo, J.; Wang, C. Sponge-like Porous Carbon/Tin Composite Anode Materials for Lithium Ion Batteries. *J. Mater. Chem.* **2012**, *22*, 9562–9567.
34. Sethuraman, V. A.; Srinivasan, V.; Bower, A. F.; Guduru, P. R. *In Situ* Measurements of Stress-Potential Coupling in Lithiated Silicon. *J. Electrochem. Soc.* **2010**, *157*, A1253–1261.
35. Sethuraman, V. A.; Chon, M. J.; Shimshak, M.; Srinivasan, V.; Guduru, P. R. *In Situ* Measurements of Stress Evolution in Silicon Thin Films during Electrochemical Lithiation and Delithiation. *J. Power Sources* **2010**, *195*, 5062–5066.
36. Sethuraman, V. A.; Srinivasan, V.; Newman, J. Analysis of Electrochemical Lithiation and Delithiation Kinetics in Silicon. *J. Electrochem. Soc.* **2013**, *160*, A394–A403.
37. Zhang, W.-J. A Review of the Electrochemical Performance of Alloy Anodes for Lithium-Ion Batteries. *J. Power Sources* **2011**, *196*, 13–24.